Full Quantum Theory for Magnon Transport in Two-sublattice Magnetic Insulators and Magnon Junctions

Tianyi Zhang[1] and Xiufeng Han[1,2,3*]
1. Beijing National Laboratory for Condensed Matter Physics, Institute of Physics, Chinese Academy of Sciences, Beijing 100190, China
2. Center of Materials Science and Optoelectronics Engineering, University of Chinese Academy of Sciences, Beijing 100049, China
3. Songshan Lake Materials Laboratory, Dongguan, Guangdong 523808, China
(Dated: August 30, 2023)

Magnons, as elementary excitations in magnetic systems, can carry and transfer angular momentum. Due to the absence of Joule heat during magnon transport, research on magnon transport has gained considerable interests over the past decade. Recently, a full quantum theory has been employed to investigate magnon transport in ferromagnetic insulators (FMIs). However, the most commonly used magnetic insulating material in experiments, yttrium iron garnet (YIG), is a ferrimagnetic insulator (FIMI). Therefore, a full quantum theory for magnon transport in FIMIs needs to be established. Here, we propose a Green's function formalism to compute the bulk and interface magnon currents in both FIMIs and antiferromagnetic insulators (AFMIs). We investigate the spatial distribution and temperature dependence of magnon currents in FIMIs and AFMIs generated by a temperature or spin chemical potential step. In AFMIs, magnon currents generated by a temperature step in the two sublattices cancel each other out. Subsequently, we numerically simulate the magnon junction effect using the Green's function formalism, and the results show a near 100% magnon junction ratio. This study demonstrates the potential of using a full quantum theory to investigate magnon transport in specific magnonic devices .

Magnons, which are the elementary excitations in magnetic systems [1–3], have potential to serve as information carriers due to their ability to carry and transfer angular momentum. Compared to electrons, using magnons for information transport offers three main advantages. Firstly, magnons can transport in magnetic insulators, which avoids the generation of Joule heat [4]. Secondly, magnons are ideal carriers for transporting GHz or THz information [5–9]. Thirdly, there are multiple methods to inject and detect magnon currents. The injection methods include microwave antennas [10–12], the spin Seebeck effect (SSE) [4, 13–16], and the spin Hall effect (SHE) [17]. The detection methods include Brillouin light scattering [18] and the inverse spin hall effect (ISHE) [19, 20]. Recently, there has been increased research on spin transport involving magnons, such as magnon-mediate drag effect [21, 22], magnon valve effect [23–26], and magnon junction effect [27]. Similar to the metal-oxide-semiconductor field-effect transistor (MOSFET) in microelectronic devices, a magnon junction, consisting of a ferromagnetic insulator (FMI1)/antiferromagnetic insulator (AFMI)/ferromagnetic insulator (FMI2), is an elementary device that controls the opening and closing of magnon transport channels. To be more specific, we can control the magnitude of the output magnon current by manipulating the magnetization state of the two FMI layers. The output magnon current is larger for the parallel state and smaller for the antiparallel state.

For a deeper understanding of the experimental phenomenon, numerous theories have been proposed to investigate magnon transport. One widely used classical equation for calculating magnon accumulation and transport [29, 30] is the LLG (Landau-Lifshitz-Gilbert) equation, initially introduced by Landau and Lifshitz, and later modified by Gilbert [28]. Another approach is the magnon Schrödinger equation, which is employed to study the wave properties and coherent transport of magnons [31–38]. The magnon Boltzmann function [39–42] is used to describe magnon transport from a particle perspective. Recently, Duine et al. proposed a Green's function formalism to elucidate magnon transport in FMIs, with and without anisotropy terms [43, 44]. The advantage of this approach lies in proposing a complete quantum theory for calculating magnon transport, facilitating the consideration of disorder and the coupling of magnons with other particles or quasi-particles. However, in experimental studies, yttrium iron garnet (YIG), a ferrimagnetic insulator (FIMI), is one of the most commonly used magnetic materials, thereby necessitating the development of a Green's function formalism specifically tailored for FIMIs.

In this paper, we present an analytical derivation of the Green's function formalism for magnon transport in FIMIs or AFMIs. Our analysis reveals the existence of two distinct effective magnon currents in FIMIs or AFMIs, which do not interact with each other. Furthermore, we investigate the spatial distribution of magnon currents induced by temperature or spin chemical potential steps in FIMIs or AFMIs. Additionally, we calculate the temperature dependence of magnon current, which is consistent with previous research [22]. Them, we study the magnon transport in a magnon junction, simulating the magnon junction effect and the result shows near

* xfhan@iphy.ac.cn

100% magnon junction ratio. Our work demonstrates the potential of utilizing the Green's function formalism to investigate magnon transport in specific magnonic devices.

The Hamiltonian for the FIMI or AFMI systems, considering Zeeman energy, nearest and next-nearest neighbor Heisenberg exchange interactions, is expressed as follows:

$$\begin{aligned}\hat{H} = & -J_{AB}\sum_{<i,m>}\hat{\boldsymbol{S}}_i\cdot\hat{\boldsymbol{S}}_m - J_A\sum_{\ll i,j\gg}\hat{\boldsymbol{S}}_{\boldsymbol{i}}\cdot\hat{\boldsymbol{S}}_j \\ & -J_B\sum_{\ll m,n\gg}\hat{\boldsymbol{S}}_m\cdot\hat{\boldsymbol{S}}_{\boldsymbol{n}} - h_{\text{ext}}\left(\sum_i\mu_A\hat{S}_i^z\right. \\ & \left.+\sum_m\mu_B\hat{S}_m^z\right)\end{aligned} \tag{1}$$

Where the subscribe $<\cdots>$ denotes summing over nearest sites, $\ll\cdots\gg$ denotes summing over next-nearest sites. $J_{AB}<0$ and $J_{A(B)}>0$ represent the nearest and next-nearest Heisenberg exchange interactions energy, respectively. $\boldsymbol{S_{i(m)}}$ is the spin in A(B) sublattice, $\mu_{A(B)}$ is the magnetic moment in A(B) sublattice. h_{ext} is applied magnetic field along the z direction. Using Holstein-Primakoff (HP) transformation [2], Fourier transformation and Bogoliubov transformation (Details in Supplemental Material [45]) we can get

$$\begin{aligned}\hat{H} = & \sum_k[\left[\frac{A_k-B_k}{2}+\frac{\sqrt{(A_k+B_k)^2-4C_k^2}}{2}\right]\hat{\alpha}_k^\dagger\hat{\alpha}_k \\ & +\left[\frac{-A_k+B_k}{2}+\frac{\sqrt{(A_k+B_k)^2-4C_k^2}}{2}\right]\hat{\beta}_k^\dagger\hat{\beta}_k]+\text{const} \\ \equiv & \sum_k(w_k^\alpha\hat{\alpha}_k^\dagger\hat{\alpha}_k+w_k^\beta\hat{\beta}_k^\dagger\hat{\beta}_k)+\text{const}\end{aligned} \tag{2}$$

where $\hat{\alpha}_k\left(\hat{\beta}_k\right),\hat{\alpha}_k^\dagger\left(\hat{\beta}_k^\dagger\right)$ are magnon annihilation and creation operators in A(B) sublattice, respectively. And $\alpha(\beta)$ mode magnons have the spin polarization direction parallel to the direction of magnetic moment in sublattice A(B). $A_k\equiv-2J_AS_A\gamma_{k,nn}-J_{AB}S_BN_n+2J_AS_AN_{nn}+h_{ext}\mu_A$, $B_k\equiv-2J_BS_B\gamma_{k,nn}-J_{AB}S_AN_n+2J_BS_BN_{nn}-h_{ext}\mu_B$, $C_k\equiv-J_{AB}\sqrt{S_AS_B}\gamma_{k,n}$, N_n, N_{nn} are the numbers of nearest and the next-nearest sites, respectively. In the case of one-dimensional atomic chain model, $N_n=N_{nn}=2$, $\gamma_{k,n}=2cos\,(ka)$, $\gamma_{k,nn}=2cos\,(2ka)$, where a is the distance between nearest sites. Thus, in both FIMI or AFMI systems, the magnon currents can be separated into two uncoupled currents with opposite polarities. Specifically, in AFMI, $J_A=J_B,S_A=S_B,\mu_A=\mu_B$, but in FIMI, the above equation does not hold.

Eq. (2) shows that in both FIMI and AFMI systems, there exist two distinct types of independent magnons. We can use Fourier transformation to Eq. (2) to transform Hamiltonian of FIMI or AFMI to the summation in coordinate space, and get

$$w_k^{\alpha(\beta)}=\sum_{n=0}^{\infty}2A_n\,(B_n)\,cos\,(nka) \tag{3}$$

Where $A_0\,(B_0)$ and $A_1\,(B_1)$ represent on-site and nearest transition energy of magnons in A(B) sublattice. Then the Hamiltonian can be written as

$$\hat{H}=\sum_{n=0}^{\infty}\sum_{i,j}\delta_{i-j\pm n}\left(A_n\hat{\alpha}_i^\dagger\hat{\alpha}_j+B_n\hat{\beta}_i^\dagger\hat{\beta}_j\right) \tag{4}$$

From Eq. (2∼4), we can see that for one-dimensional atomic chain model $A_{2i+1}=B_{2i+1}=0(i=0,1,2\cdots)$. Then we investigate the variation of the Fourier expansion coefficient with expansion order, as shown in Fig. 1, where for AFMI we use the following parameters [46, 47]: $J_{AB}=-0.002$ eV, $J_A=J_B=0.02$ eV, $S_A=S_B=1$, and for FIMI we use the following parameters [30]: $J_{AB}=-0.005$ eV, $J_A=0.05$ eV, $J_B=0.01$ eV,$S_A=1$, $S_B=1.5$. We can see that for both AFMI and FIMI the odd parts of the expansion coefficients are consistently 0, while the even parts approach 0 when n $\geq$ 4, indicating that only two terms $A_0\,(B_0)$ and $A_2\,(B_2)$ need to be retained.

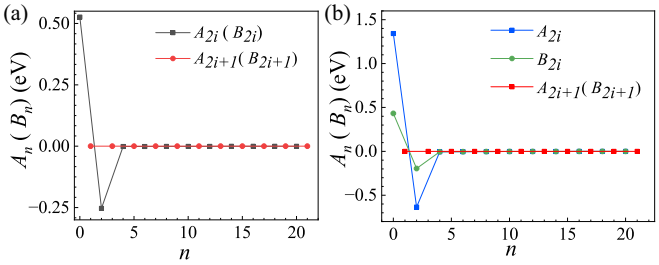

FIG. 1. The variation of the Fourier expansion coefficient with expansion order n for (a) AFMI and (b) FIMI.The parameters are shown as follows, (a) $J_{AB}=-0.002$ eV, $J_A=J_B=0.02$ eV, $S_A=S_B=1$ and (b) $J_{AB}=-0.005$ eV, $J_A=0.05$ eV, $J_B=0.01$ eV, $S_A=1$, $S_B=1.5$.

Next, we investigate the magnon transport in FIMI or AFMI systems, considering only two terms $A_0\,(B_0)$ and $A_2\,(B_2)$. Fig. 2 presents a schematic diagram depicting the magnon current transport through FIMI or AFMI. The FIMI or AFMI is connected to two normal metals (NMs) with temperatures T_R, T_L and spin chemical potentials μ_L, μ_R, respectively. The magnon current arises from the temperature or spin chemical potential difference between two NMs. To compute the bulk magnon current, we first calculate the retarded and advanced Green's functions using the Dyson equation

$$\mathcal{G}^{R(A)}(\varepsilon)=\left[\varepsilon^{+(-)}-H-\hbar\Sigma^{R(A)}\,(\varepsilon)\right]^{-1} \tag{5}$$

Where $\mathcal{G}^{R(A)}$ is retarded (advanced) Green's function, $\varepsilon^{+(-)}=\varepsilon+(-)i\eta$, η is a infinitesimal positive number, H is Hamiltonian for the FIMI or AFMI systems, and $\Sigma^{R(A)}\,(\varepsilon)$ is retarded(advanced) self-energy, which describes the coupling between FIMI or AFMI and external environment. According to Eq. (4), considering the first two terms of the expansion, the Hamiltonian for the FIMI or AFMI systems is

$$\hat{H}=\sum_{i,j}[(A_0\delta_{i,j}+A_2\delta_{i,j\pm2})\hat{\alpha}_i^\dagger\hat{\alpha}_j+(B_0\delta_{i,j}+B_2\delta_{i,j\pm2})\hat{\beta}_i^\dagger\hat{\beta}_j] \tag{6}$$

and the self-energy is composed of three items $\Sigma^R\,(\varepsilon)=$

FIG. 2. Schematic diagram that illustrates the transport of magnon current through FIMI or AFMI driven by temperature or spin chemical potential step.

$\Sigma_C^R(\varepsilon)+\Sigma_L^R(\varepsilon)+\Sigma_R^R(\varepsilon)$, where

$$\begin{aligned}\Sigma_{C\ i,j}^R(\varepsilon) &= -i\alpha(\varepsilon-\mu_C)\delta_{i,j}/\hbar,\\ \Sigma_{L\ i,j}^R(\varepsilon) &= -i\eta^L(\varepsilon-\mu_L)\delta_{i,j}(\delta_{j,1}+\delta_{j,2})/\hbar,\\ \Sigma_{R\ i,j}^R(\varepsilon) &= -i\eta^R(\varepsilon-\mu_R)\delta_{i,j}(\delta_{j,N}+\delta_{j,N-1})/\hbar\end{aligned} \tag{7}$$

are retarded self-energy induced by Gilbert damping in FIMI or AFMI, connection with left NM and right NM, respectively. Where α is Gilbert damping constant, $\hbar$ is reduced Planck's constant, $\eta^{L(R)}$ is parameter that represents the coupling with left and right NMs [44, 48], $\mu_{L(R)}$ is spin chemical potential of left(right) NM, μ_C is magnon potential of FIMI or AFMI.

Secondly, we can calculate the magnon density matrix using Langreth rule, take α mode magnon as an example [44]

$$\rho \equiv <\hat{\alpha}^\dagger\hat{\alpha}> = \int_{-\infty}^{\infty}\frac{d\varepsilon}{2\pi}\left[\mathcal{G}^R(\varepsilon)\, i\hbar\Sigma^<(\varepsilon)\,\mathcal{G}^A(\varepsilon)\right] \tag{8}$$

where the lesser self-energy can be calculated by

$$\begin{aligned}\Sigma^<(\varepsilon) &= \Sigma_C^<(\varepsilon)+\textstyle\sum_{r\in\{L,R\}}\Sigma_r^<(\varepsilon)\\ &= 2iN_B\left(\tfrac{\varepsilon-\mu_C}{k_BT_C}\right)Im\left(\Sigma_C^R(\varepsilon)\right)\\ &+\textstyle\sum_{r\in\{L,R\}}2iN_B\left(\tfrac{\varepsilon-\mu_r}{k_BT_r}\right)Im\left(\Sigma_r^R(\varepsilon)\right)\end{aligned} \tag{9}$$

Where $N_B(x)=\frac{1}{e^x-1}$ is Bose-Einstein distribution. Then we can calculate bulk magnon current using Heisenberg motion equation.

$$\hbar\frac{d<\alpha_i^\dagger\alpha_i>}{dt} = \sum_j -i\left(h_{i,j}\rho_{j,i}-h_{j,i}\rho_{i,j}\right) = \sum_j j_{m;i,j} \tag{10}$$

where $j_{m;i,j}$ represents the magnon current from site i to site j, $h_{i,j}=A_0\delta_{i,j}+A_2\delta_{i,j\pm2}$ is Hamiltonian for α mode magnons. Eq. (10) indicates that the change of the magnon number at site i is equal to all magnon currents from site i to other sites.

According to [22], The reversal of the FM layer magnetization does not affect the transport of magnon generated by the spin Hall effect (SHE). However, for magnon current induced by the spin Seebeck effect (SSE), the reversal of the FM layer magnetization leads to a opposite output signal. Therefore, we assume that magnons with opposite polarity experience an equivalent spin chemical potential step but an opposite temperature gradient.

The Green's function formalism can also be utilized to calculate the interface magnon current. By using the Landauer-Büttiker formula [44], we find that the magnon current at the interface between AFMI and NMs can be expressed as follows:

$$\begin{aligned}j_{L(R)}^m &= j_{L(R),\alpha}^m + j_{L(R),\beta}^m\\ &= \int\tfrac{d\varepsilon}{2\pi}\left[N_B\left(\tfrac{\varepsilon-\mu_{L(R)}}{k_BT_{L(R)}}\right)-N_B\left(\tfrac{\varepsilon-\mu_{R(L)}}{k_BT_{R(L)}}\right)\right]T_{b,\alpha}(\varepsilon)\\ &+\int\tfrac{d\varepsilon}{2\pi}\left[N_B\left(\tfrac{\varepsilon-\mu_{L(R)}}{k_BT_{L(R)}}\right)-N_B\left(\tfrac{\varepsilon-\mu_C}{k_BT_{AFMI}}\right)\right]T_{f,\alpha}(\varepsilon)\\ &+\int\tfrac{d\varepsilon}{2\pi}\left[N_B\left(\tfrac{\varepsilon-\mu_{L(R)}}{k_BT_{R(L)}}\right)-N_B\left(\tfrac{\varepsilon-\mu_{R(L)}}{k_BT_{L(R)}}\right)\right]T_{b,\beta}(\varepsilon)\\ &+\int\tfrac{d\varepsilon}{2\pi}\left[N_B\left(\tfrac{\varepsilon-\mu_{L(R)}}{k_BT_{AFMI}}\right)-N_B\left(\tfrac{\varepsilon-\mu_C}{k_BT_{L(R)}}\right)\right]T_{f,\beta}(\varepsilon)\}\end{aligned} \tag{11}$$

Where the transmission function

$$\begin{aligned}T_{b,i}(\varepsilon) &\equiv Tr\left[\hbar\Gamma_{L(R),i}(\varepsilon)\,\mathcal{G}_i^R(\varepsilon)\,\hbar\Gamma_{R(L),i}(\varepsilon)\,\mathcal{G}_i^A(\varepsilon)\right],\\ T_{f,i}(\varepsilon) &\equiv Tr\left[\hbar\Gamma_{L(R),i}(\varepsilon)\,\mathcal{G}_i^R(\varepsilon)\,\hbar\Gamma_{AFMI,i}(\varepsilon)\,\mathcal{G}_i^A(\varepsilon)\right]\end{aligned} \tag{12}$$

Where $i=\alpha$ *or* β, are two modes of magnons with opposite polarity, the rates $\Gamma_{L(R),i}(\varepsilon)=-2Im\left(\Sigma_{L(R),i}^R(\varepsilon)\right)$.

The Green's function formalism can be utilized to calculate magnon current driven by temperature gradient or spin chemical potential gradient. In particular, we use temperature difference between left and right NMs to simulate magnon current excited by SEE, and use spin chemical difference between left and right NMs to simulate magnon current excited by SHE.

To investigate the spatial distribution and temperature dependence of magnon currents in AFMI excited by the SSE and the SHE, we set the temperature difference ΔT and spin chemical potential difference $\Delta\mu$ between two NMs. In Fig. 3. (a), we calculated spatial distribution of magnon currents excited by SSE in AFMI. The parameters used in simulation are set to be $A_0=B_0=0.5$ eV, $A_2=B_2=-0.25$ eV, $N=100$, $h_{ext}=0$, $\mu_L=\mu_R=0$, $\eta^L=\eta^R=8$, $k_BT_{AFMI}=0.026$ eV, $T_L=1.2\,T_{AFMI}$, $T_R=0.8\,T_{AFMI}$, $\mu_{AFMI}=0$ and $\alpha_{AFMI}=0.001$ [49]. We can see that the magnon currents composed of α and β modes magnons have different sign but the same absolute value, so the α and β mode magnon currents cancel with each other, total magnon current j_m^{sum} is 0. Then we keep the temperature of left NM $T_L=1.2\,T_{AFMI}$ fixed, change the temperature of right NM T_R, and average all the α mode magnon current at 100 sites, the temperature dependence of averaged α mode magnon currents $\bar{j}_m^\alpha$ is shown in Fig. 3. (b), we can see that $\bar{j}_m^\alpha$ shows positive correlation dependence on temperature difference between left and right NMs $\Delta T=T_L-T_R$ and the influence of ΔT on $\bar{j}_m^\alpha$ is gradually reduced as ΔT increases. Then we calculated spatial distribution of magnon currents excited by SHE in AFMI, see Fig. 3. (c). Spin chemical potential $\mu_L=0.1A_0$, $\mu_R=0$, temperature

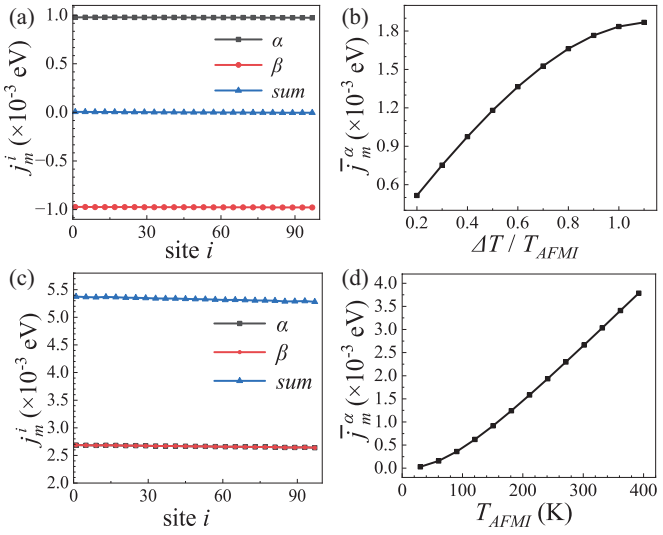

FIG. 3. Spatial distribution and temperature dependence of magnon currents excited by SSE (a, b) and SHE (c, d) in AFMI. The spin chemical potential of two normal metals and temperature profile are set to be (a) $\mu_L = \mu_R = 0$, $k_BT_{AFMI} = 0.026$ eV, $T_L = 1.2\ T_{AFMI}$, $T_R = 0.8\ T_{AFMI}$, and (c) $\mu_L = 0.1A_0$, $\mu_R = 0$, $k_BT_{AFMI} = 0.026$ eV, $T_L = T_R = T_{AFMI}$

$k_BT_{AFMI} = 0.026$ eV, $T_L = T_R = T_{AFMI}$. We can see that for magnon current excited by SHE, α and β mode magnons contribute equally in the component of sum magnon currents. And then we change the temperature of left NM, AFMI and right NM at the same time, and calculate the temperature dependence of average α mode magnon current, as shown in Fig. 3. (d). We can see that $\bar{j}_m^{\alpha}$ increases as T_{AFMI} increases. It can be explained by that as T_{AFMI} increase, the number of α mode magnon in sublattice $n_\alpha(\varepsilon) = \frac{1}{e^{\frac{\varepsilon}{k_BT_{AFMI}}}-1}$ increases, therefore, the magnons involved in transport increase.

Then we calculate the spatial distribution and temperature dependence of magnon currents in FIMI excited by the SSE and the SHE. In Fig. 4. (a), we calculated spatial distribution of magnon currents excited by SSE in FIMI. The parameters used in simulation are set to be $A_0 = 1.3$ eV, $B_0 = 0.43$ eV, $A_2 = -0.6$ eV, $B_2 = -0.2$ eV, N = 100, $h_{ext} = 0$, $\mu_L = \mu_R = 0$, $\eta^L = \eta^R = 8$, $k_BT_{FIMI} = 0.026$ eV, $T_L = 1.2\ T_{FIMI}$, $T_R = 0.8\ T_{FIMI}$, $\mu_{FIMI} = 0$ and $\alpha_{FIMI} = 0.001$. We can see that although magnon currents generated by α and β mode magnons have opposite sign, they do not cancel with each other. Then we keep left NM temperature $T_L = 1.2\ T_{FIMI}$ fixed, change the right NM temperature T_R, calculate the site average magnon current $\bar{j}_m^{\alpha}$, $\bar{j}_m^{\beta}$, $\bar{j}_m^{sum}$ dependence on the temperature difference, see Fig. 4. (b) we can see the absolute value of $\bar{j}_m^{\alpha}$, $\bar{j}_m^{\beta}$, $\bar{j}_m^{sum}$ increase as temperature difference between left and right NMs ΔT increases. As for magnon current excited by SHE in FIMI, we set parameters to be spin chemical potential $\mu_L = 0.1A_0$, $\mu_R = 0$, temperature $k_BT_{FIMI} = 0.026$ eV, $T_L = T_R = T_{FIMI}$, and calculate the space distribution of magnon current. We can see from Fig. 4. (c) that in FIMI due to the difference of on-site and next-nearest transition energy between α and β mode magnons, the magnon currents composed by these two types of magnons are not the same. And then we change the temperature of the whole system at the same time, and calculate the temperature dependence of average magnon current $\bar{j}_m^{\alpha}$, $\bar{j}_m^{\beta}$, $\bar{j}_m^{sum}$. We can see from Fig. 4. (d) that $\bar{j}_m^{\alpha}$, $\bar{j}_m^{\beta}$, $\bar{j}_m^{sum}$ all increase as system temperature increase, which is due to the increase of magnons in two sublattices.

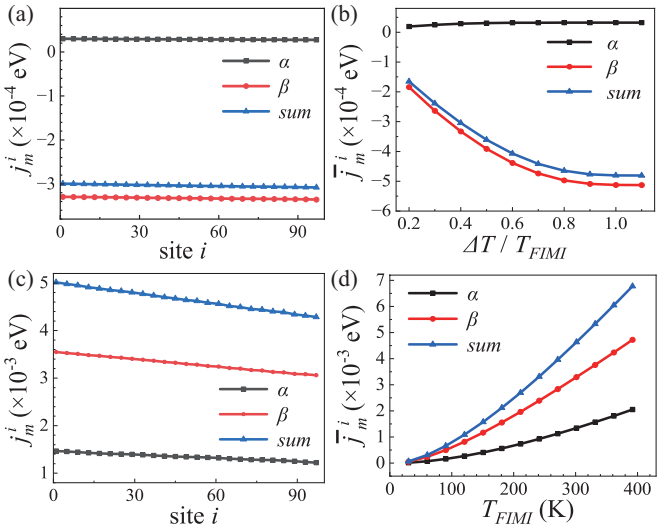

FIG. 4. Spatial distribution and temperature dependence of magnon currents excited by SSE (a, b) and SHE (c, d) in FIMI.The spin chemical potential of two normal metals and temperature profile are set to be (a) $\mu_L = \mu_R = 0$, $k_BT_{FIMI} = 0.026$ eV, $T_L = 1.2T_{FIMI}$, $T_R = 0.8T_{FIMI}$, and (c) $\mu_L = 0.1A_0$, $\mu_R = 0$, $k_BT_{FIMI} = 0.026$ eV, $T_L = T_R = T_{FIMI}$

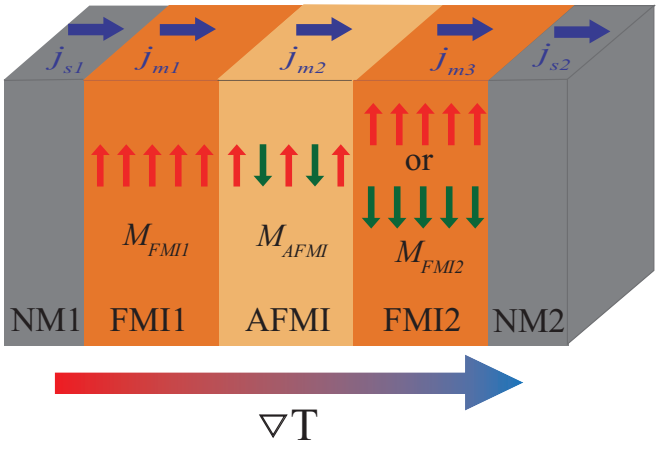

FIG. 5. Schematic diagram of magnon current driven by temperature gradient transporting through a magnon junction.

Using the same method above, we can calculate magnon currents in magnon junction, the model includes a magnon junction and two NM leads, as shown in Fig. 5. The boundary conditions are set to be that magnon currents are continuous at interface between FMI1 and AFMI1, between AFMI and FMI2. And the magnon current injected from NM1 to FMI1 is set to be zero, which excluded the influence of spin current injected from NM1 on output magnon current (Details of calculation are in Supplemental Material [45]).

For parallel magnetization, magnon potentials are $\mu_{FMI1} = 20$ meV, $\mu_{AFMI} = 5.3$ meV, $\mu_{FMI2} = 18$ meV, and the magnon current at the interface of FMI2 and NM2 is 6.53×10^{-4} eV; for antiparallel magnetization state, magnon potentials are $\mu_{FMI1} = -37$ meV, $\mu_{AFMI} = 5.2$ meV, $\mu_{FMI2} = -36.8$ meV, and the magnon current at the interface of FMI2 and NM2 is 4.79×10^{-7} eV. It shows near 100% magnon junction ratio, here magnon junction ratio is MJR $= (J_{m,\uparrow\uparrow} - J_{m,\uparrow\downarrow})/(J_{m,\uparrow\uparrow}+J_{m,\uparrow\downarrow})$, where $J_{m,\uparrow\uparrow}$ and $J_{m,\uparrow\downarrow}$ are output magnon current of parallel magnetization and antiparallel magnetization state.

In conclusion, we propose a Green's function formalism as a comprehensive quantum theory for investigating magnon transport in AFMIs or FIMIs, specifically tailored for two-sublattice magnetic systems. We studied the spatial distribution and temperature dependence of the magnon current induced by temperature or spin chemical potential step in FIMIs or AFMIs. Our results reveal that the magnon currents in both sublattices exhibit a positive correlation with temperature. Interestingly, in AFMI, the magnon currents generated by temperature step in the two sublattices cancel each other out. Furthermore, we numerically simulate the magnon junction effect using the Green's function formalism, which yields a near 100% magnon junction ratio. Our work demonstrates the potential of employing comprehensive quantum theory to unravel the intricacies of magnon transport in specific magnonic devices.

This work is financial supported by the National Key Research and Development Program of China (MOST) (Grant No. 2022YFA1402800), the National Natural Science Foundation of China (NSFC) (Grant No. 51831012, 12134017), and partially supported by the Strategic Priority Research Program (B) (Grant No. XDB33000000).

[1] A.V. Chumak, V.I. Vasyuchka, A.A. Serga, and B. Hillebrands, Magnon spintronics, Nature Physics **11**, 453 (2015).
[2] H. Y. Yuan, Y. Cao, A. Kamra, R. A. Duine, and P. Yan, Quantum magnonics: When magnon spintronics meets quantum information science, Physics Reports **965**, 1 (2022).
[3] F. Bloch, Zur theorie des ferromagnetismus, Zeitschrift für Physik **61**, 206 (1930).
[4] J. Xiao, G. E. W. Bauer, K.-c. Uchida, E. Saitoh, and S. Maekawa, Theory of magnon-driven spin seebeck effect, Physical Review B **81**, 214418 (2010).
[5] J. D. Adam, Analog signal processing with microwave magnetics, Proceedings of the IEEE **76**, 159 (1988).
[6] V. Cherepanov, I. Kolokolov, and V. L"Vov, The saga of yig: Spectra, thermodynamics, interaction and relaxation of magnons in a complex magnet, Physics Reports **229**, 81 (1993).
[7] J. M. Owens, J. H. Collins, and R. L. Carter, System applications of magnetostatic wave devices, Circuits Systems and Signal Processing **4**, 317 (1985).
[8] T. Balashov, P. Buczek, L. Sandratskii, A. Ernst, and W. Wulfhekel, Magnon dispersion in thin magnetic films, J Phys Condens Matter **26**, 394007 (2014).
[9] T. H. Chuang, K. Zakeri, A. Ernst, Y. Zhang, H. J. Qin, Y. Meng, Y. J. Chen, and J. Kirschner, Magnetic properties and magnon excitations in fe(001) films grown on ir(001), Phys.rev.b **89**, 1493 (2014).
[10] T. Schneider, A. A. Serga, T. Neumann, B. Hillebrands, and M. P. Kostylev, Phase reciprocity of spin-wave excitation by a microstrip antenna, Physical Review B **77**, 214411 (2008).
[11] M. Jamali, J. H. Kwon, S. M. Seo, K. J. Lee, and H. Yang, Spin wave nonreciprocity for logic device applications, Sci Rep **3**, 3160 (2013).
[12] Vladislav, E., Demidov, Mikhail, P., Kostylev, Karsten, Rott, Patryk, and Krzysteczko, Excitation of microwaveguide modes by a stripe antenna, Applied Physics Letters **95**, 257202 (2009).
[13] J.-i. Ohe, H. Adachi, S. Takahashi, and S. Maekawa, Numerical study on the spin seebeck effect, Physical Review B **83**, 115118 (2011).
[14] G. E. W. Bauer, E. Saitoh, and B. J. van Wees, Spin caloritronics, Nature Materials **11**, 391 (2012).
[15] H. Yu, S. D. Brechet, and J.-P. Ansermet, Spin caloritronics, origin and outlook, Physics Letters A **381**, 825 (2017).
[16] S. M. Rezende, R. Rodrguez-Surez, R. O. Cunha, A. R. Rodrigues, F. Machado, G. Guerra, J. Ortiz, and A. Azevedo, Magnon spin-current theory for the longitudinal spin-seebeck effect, Physical Review B (2014).
[17] J. Sinova, S. O. Valenzuela, J. Wunderlich, C.H Back, and T. Jungwirth, Spin hall effects, Reviews of Modern Physics **87**, 1213 (2015).
[18] S. O. Demokritov, B. Hillebrands, and A. N. Slavin, Brillouin light scattering studies of confined spin waves: linear and nonlinear confinement, Physics Reports **348**, 441 (2001).
[19] L. K. Werake, B. A. Ruzicka, and H. Zhao, Observation of intrinsic inverse spin hall effect, Physical Review Letters **106**, 107205 (2011).
[20] Saitoh, E., Ueda, M., Miyajima, H., Tatara, and G., Conversion of spin current into charge current at room temperature: Inverse spin-hall effect, Applied Physics Letters **88**, 182509 (2006).
[21] S. S. Zhang and S. Zhang, Magnon mediated electric current drag across a ferromagnetic insulator layer, Phys Rev Lett **109**, 096603 (2012).

[22] H. Wu, C. H. Wan, X. Zhang, Z. H. Yuan, Q. T. Zhang, J. Y. Qin, H. X. Wei, X. F. Han, and S. Zhang, Observation of magnon-mediated electric current drag at room temperature, Physical Review B **93**, 10.1103/PhysRevB.93.060403 (2016).

[23] H. Wu, L. Huang, C. Fang, B. S. Yang, C. H. Wan, G. Q. Yu, J. F. Feng, H. X. Wei, and X. F. Han, Magnon valve effect between two magnetic insulators, Phys Rev Lett **120**, 097205 (2018).

[24] L.J Cornelissen, J. Liu, B.J van Wees, and R.A Duine, Spin-current-controlled modulation of the magnon spin conductance in a three-terminal magnon transistor, Physical Review Letters **120**, 097702 (2018).

[25] J. Cramer, F. Fuhrmann, U. Ritzmann, V. Gall, T. Niizeki, R. Ramos, Z. Qiu, D. Hou, T. Kikkawa, J. Sinova, U. Nowak, E. Saitoh, and M. Klui, Magnon detection using a ferroic collinear multilayer spin valve, Nature Communications **9**, 1089 (2018).

[26] J. Zheng, A. Rückriegel, S. A. Bender, and R. A. Duine, Ellipticity and dissipation effects in magnon spin valves, Physical Review B **101**, 10.1103/PhysRevB.101.094402 (2020).

[27] C. Y. Guo, C. H. Wan, X. Wang, C. Fang, P. Tang, W. J. Kong, M. K. Zhao, L. N. Jiang, B. S. Tao, G. Q. Yu, and X. F. Han, Magnon valves based on yig/nio/yig all-insulating magnon junctions, Physical Review B **98**, 10.1103/PhysRevB.98.134426 (2018).

[28] T. L. Gilbert, Classics in magnetics a phenomenological theory of damping in ferromagnetic materials, IEEE Transactions on Magnetics **40**, 3443 (2004).

[29] U. Ritzmann, D. Hinzke, and U. Nowak, Propagation of thermally induced magnonic spin currents, Physical Review B **89**, 10.1103/PhysRevB.89.024409 (2014).

[30] U. Ritzmann, D. Hinzke, and U. Nowak, Thermally induced magnon accumulation in two-sublattice magnets, Physical Review B **95**, 10.1103/PhysRevB.95.054411 (2017).

[31] P. Yan, X. S. Wang, and X. R. Wang, All-magnonic spin-transfer torque and domain wall propagation, Phys. Rev. Lett. **107**, 177207 (2011).

[32] W. Wang, M. Albert, M. Beg, M.-A. Bisotti, D. Chernyshenko, D. Cortés-Ortuño, I. Hawke, and H. Fangohr, Magnon-driven domain-wall motion with the dzyaloshinskii-moriya interaction, Phys. Rev. Lett. **114**, 087203 (2015).

[33] J. Lan, W. Yu, R. Wu, and J. Xiao, Spin-wave diode, Phys. Rev. X **5**, 041049 (2015).

[34] C. Jia, D. Ma, A. F. Schffer, and J. Berakdar, Twisted magnon beams carrying orbital angular momentum, Nature Communications **10**, 2077 (2019).

[35] W. Yu, J. Lan, R. Wu, and J. Xiao, Magnetic snell's law and spin-wave fiber with dzyaloshinskii-moriya interaction, Phys. Rev. B **94**, 140410 (2016).

[36] Y. W. Xing, Z. R. Yan, and X. F. Han, Magnon valve effect and resonant transmission in a one-dimensional magnonic crystal, Phys. Rev. B **103**, 054425 (2021).

[37] Z. Wang, Y. Cao, and P. Yan, Goos-hänchen effect of spin waves at heterochiral interfaces, Phys. Rev. B **100**, 064421 (2019).

[38] S.-J. Lee, J.-H. Moon, H.-W. Lee, and K.-J. Lee, Spin-wave propagation in the presence of inhomogeneous dzyaloshinskii-moriya interactions, Phys. Rev. B **96**, 184433 (2017).

[39] A. Manchon and S. Zhang, Theory of nonequilibrium intrinsic spin torque in a single nanomagnet, Physical Review B **78**, 10.1103/PhysRevB.78.212405 (2008).

[40] L. J. Cornelissen, K. J. H. Peters, G. E. W. Bauer, R. A. Duine, and B. J. van Wees, Magnon spin transport driven by the magnon chemical potential in a magnetic insulator, Physical Review B **94**, 10.1103/PhysRevB.94.014412 (2016).

[41] T. Liu, W. Wang, and J. Zhang, Collective induced antidiffusion effect and general magnon boltzmann transport theory, Physical Review B **99**, 10.1103/PhysRevB.99.214407 (2019).

[42] J. Sinova, D. Culcer, Q. Niu, N. A. Sinitsyn, T. Jungwirth, and A. H. MacDonald, Universal intrinsic spin hall effect, Phys Rev Lett **92**, 126603 (2004).

[43] W. P. Sterk, H. Y. Yuan, A. Rckriegel, B. Z. Rameshti, and R. A. Duine, Green's function formalism for nonlocal elliptical magnon transport, Physical Review B **104**, 10.1103/PhysRevB.104.174404 (2021).

[44] J. Zheng, S. Bender, J. Armaitis, R. E. Troncoso, and R. A. Duine, Green's function formalism for spin transport in metal-insulator-metal heterostructures, Physical Review B **96**, 10.1103/PhysRevB.96.174422 (2017).

[45] See supplemental material at the end of manuscript., .

[46] D. Ködderitzsch, W. Hergert, W. M. Temmerman, Z. Szotek, A. Ernst, and H. Winter, Exchange interactions in nio and at the nio(100) surface, Phys. Rev. B **66**, 064434 (2002).

[47] W.-B. Zhang, Y.-L. Hu, K.-L. Han, and B.-Y. Tang, Pressure dependence of exchange interactions in NiO, Phys. Rev. B **74**, 054421 (2006).

[48] Y. Tserkovnyak, A. Brataas, and G. E. Bauer, Enhanced gilbert damping in thin ferromagnetic films, Phys Rev Lett **88**, 117601 (2002).

[49] T. Moriyama, K. Hayashi, K. Yamada, M. Shima, Y. Ohya, and T. Ono, Intrinsic and extrinsic antiferromagnetic damping in nio, Phys. Rev. Mater. **3**, 051402 (2019).

[50] V. Baltz, A. Manchon, M. Tsoi, T. Moriyama, T. Ono, and Y. Tserkovnyak, Antiferromagnetic spintronics, Reviews of Modern Physics **90**, 015005 (2018).

[51] M. V. Costache, M. Sladkov, S. M. Watts, C. Wal, and B. Wees, Electrical detection of spin pumping due to the precessing magnetization of a single ferromagnet, Physical Review Letters **97**, 216603 (2006).

[52] K.-S. Lee, S.-W. Lee, B.-C. Min, and K.-J. Lee, Threshold current for switching of a perpendicular magnetic layer induced by spin hall effect, Applied Physics Letters **102**, 10.1063/1.4798288 (2013).

[53] Y. W. Xing, Z. R. Yan, and X. F. Han, Comparison of spin-wave transmission in parallel and antiparallel magnetic configurations, Physical Review B **105**, 064427 (2022).

[54] J. Barker and G. E. W. Bauer, Thermal spin dynamics of yttrium iron garnet, Phys. Rev. Lett. **117**, 217201 (2016).

[55] L.-S. Xie, G.-X. Jin, L. He, G. E. W. Bauer, J. Barker, and K. Xia, First-principles study of exchange interactions of yttrium iron garnet, Phys. Rev. B **95**, 014423 (2017).